


Porosity detection by analyzing arc sound signal acquired during the welding process of gas pipeline steel

M. F. M. Yusof¹  · M. A. Kamaruzaman¹ · M. Ishak¹ · M. F. Ghazali¹

Received: 30 March 2016 / Accepted: 15 August 2016 / Published online: 24 August 2016
© Springer-Verlag London 2016

Abstract Detection of severe defects such as porosity underneath the weld bead during the welding process is vital during installation of a gas pipeline network because such defects might lead to fatigue crack. In this study, the work associated with detection of porosity through analysis of the acquired arc sound is presented. Air-borne acoustic signal was acquired during the metal inert gas welding process on API 5L X70 gas pipeline steel. Then, the acquired signal was analyzed using Hilbert Huang transform (HHT), which uses empirical mode decomposition for the purpose of filtering unrelated-to-damage signal components, and Hilbert spectral analysis to obtain the energy-frequency-distance plot. Results showed a significant energy amplitude pattern at the region where both surface- and subsurface-pores existed. Thus, the application of HHT analysis to the acquired arc sound signal has significantly assisted in identifying hidden information that is related to the existence of defects. This finding would enhance the development of an online welding defect detection system during the welding process.

Keywords Porosity · Metal-inert gas welding · Arc sound · Hilbert-Huang transform

1 Introduction

Welding is one of the major joining methods in installation of a gas pipeline network. Therefore, it is an essential process and must be carried out properly prior to the commissioning stage to ensure that the joining strength has been considered. This aspect is vital because failure in a pipeline system can lead to a massive impact to public safety and economy, as well as result in damage to the environment [1]. Many incidents of failures in pipeline systems have been reported since the last couple of decades. With the exception of failures caused by corrosion problem, many studies suggested that most pipeline failures begun with crack initiation from defects, such as burnt through [2], lack of penetration [3], and subsurface pores [4], in the weld bead area. Although a precautionary action is taken by performing the welding process according to the standard procedures during the installation, these defects can still exist as a result of several uncertainties during the process. Thus, welding inspection must be conducted to ensure that the quality and strength of the welded joint are adequate or more than enough before operation of a pipeline system.

During the inspection process, several types of defects that are visible on the weld bead surface can easily be identified through visual inspection or nondestructive testing approaches, such as liquid penetration test and magnetic particle method. Meanwhile, various methods such as acoustic emission, ultrasonic testing, and X-ray radiography are needed for detection of severe subsurface defects, such as cavity, linear porosity, gas pores, and slag inclusion. In 1990, Carlson et al. [5] showed that the use of ultrasonic testing can significantly aid detection of incomplete and side-wall penetration, as well as porosity underneath a weld bead. In another earlier work [6], this method was employed

✉ M. F. M. Yusof
fadhlan@ump.edu.my

¹ Faculty of Mechanical Engineering, University Malaysia Pahang, Pahang, Malaysia

to access the integrity of spot weld. However, the application of ultrasonic testing can only provide information under the vicinity of the scanned area, and this method is time-consuming when used to measure larger areas. Contrary to ultrasonic testing, acoustic emission technique provides a more global measurement with the use of an array of sensors. Apart from detecting the subsurface defect beneath the welding bead [7], this method is an ideal method to locate the position of defects [8]. However, this method has its own limitations when applied in hardly-accessed area because of the structure-borne nature of the signal, in which the sensor needs to form contact with the surface of the measured area. In another approach, X-ray radiography has been used to detect subsurface defects, such as porosity [9–11] and inclusion [10, 12]. Nevertheless, in some cases, this method can be subjective and time-consuming [9]. Other researchers [13, 14] demonstrated the use of the arc spectra in the detection of porosity and other types of defect.

The feasibility of many methods has been studied to establish facile and cost-effective method to identify defects on weld bead. As previously presented, each method offers advantages and disadvantages. Unlike other methods, the use of arc sound in detection of defects can be considered as cost-effective and promotes non-contact measurement. As a result, this method has attracted considerable research interest. Previous studies showed that analysis of acoustic signal acquired during the welding process significantly aided the monitoring of certain characteristics, such as penetration quality [15, 16], weld pool status [17], irregularities, and stability [18], during the welding process.

Basically, detection of defects by sound signal analysis is based on the understanding of several phenomena, such as weld pool oscillation behavior [17, 19], arc plasma jet pulsation [15], change in arc intensity [17], and metal transfer [18], which are the possible sources of sound generated during the welding process. Nonetheless, it is important to understand that sound signals can also be created by non-damage-related sources. According to You et al. [20], an acquired sound is subject to interference from background noise under harsh surrounding. Thus, in many studies, the application of the signal processing method has been significant in addressing problems associated with the presence of non-damage-related sources of sound signals. On one hand, in some applications that associated with noise problem, the signal processing method is used to decompose the signal into several components to reveal the defect-related component. For instance, Wang et al. [19] demonstrated the use of the short-time Fourier transform in detecting and locating irregularities on a weld bead. Meanwhile, on the other hand, instead of decomposing the signal, the signal processing method is used to extract significant signal features which

lead to defect detection. In works related to this approach, Wang and Zhao [15] used the variance of a segmented sound signal as a feature to monitor a keyhole opening. This feature was found to give a significant correlation with keyhole size, which can be utilized to monitor burn-through defects. Moreover, Huang and Kovacevic [21] extracted the sound pressure deviation and band power to establish the relation between acoustic signal and depth of penetration in laser welding through artificial neural network. Saad et al. [17] extracted the power spectral density of the segmented sound signal acquired from the welding process. This feature has been used as an input for a neural network model to distinguish the keyhole mode from the cutting mode. By establishing the distinction between sounds from both modes, monitoring the keyhole phenomena during the welding process is easier. In another research, Grad et al. [18] found that kurtosis of sound signal can be used as a sensitive feature to monitor the stability of a welding process. Moreover, time delay from acquired sound signals has been used to locate defects in weld bead [22].

Previous research demonstrated that the use of sound signal can provide a significant result in detecting several types of defect, as well as in monitoring certain phenomena during the welding process to prevent defect formation. This detection method would realize the development of a welding monitoring system to control the welding process. However, evaluation of methods based on sound signal analysis is limited to several types of defect. This method has shown great promise in the detection of a wide variety of defects, especially the more severe types, such as porosity and inclusion underneath the weld bead. Moreover, an in-depth understanding on noise elimination methods is necessary before a real-time monitoring technology using arc sound can be established.

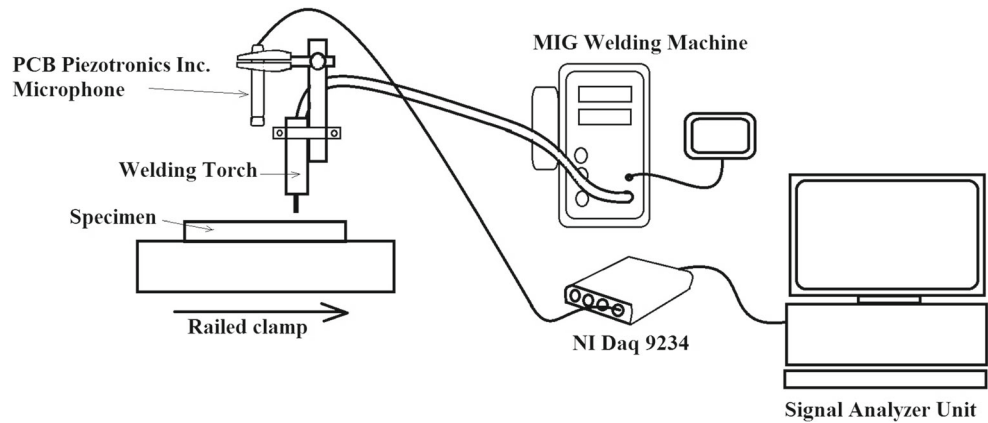
In this study, the work associated with detection and localization of porosity through sound signal analysis is presented. Sound signal was acquired during the metal-inert gas (MIG) welding process of API 5L X70 steel. To reveal the presence of defects, the obtained sound signals were processed using Hilbert-Huang transform (HHT), which included empirical mode decomposition (EMD) and Hilbert spectral analysis (HSA) as decomposition and post-processing methods, respectively.

2 Methodology

2.1 Experimental setup

The arrangement of instruments in this experiment is shown in Fig. 1. The instrumentation system consisted of

Fig. 1 Experimental setup



a PCB Piezotronic Inc. microphone with bandwidth of 20 to 10,000 Hz, a National Instrument analog-to-digital converter model NI9234, and a PC as a signal analyzer unit. In the data acquisition process, the arc sound was sampled at a rate of 25.6 kSamples/s . In this experiment, API 5L X70 grade carbon steel specimens (40 mm x 70 mm x 4 mm) were used. The welding parameters were set according to values shown in Table 1.

During the welding process, the specimen on the railed clamp moved in accordance to the welding speed, which was set in the beginning stage. Meanwhile, the microphone was attached to the welding torch to ensure that the distance from the area of metal transfer was kept constant.

2.2 Signal analysis

In principle, HHT uses EMD, as a decomposition method, and HSA to obtain the energy amplitude distribution in time-frequency space. According to Huang et al. [23], the algorithms of EMD are as follows:

1. Find both local extrema and local minima of the acquired time series signal $x(t)$.
2. Envelop the acquired signal by plotting the local extrema and minima. In this case, the plot of local extrema is called upper envelop ($max[x(t)]$), whereas the plot of local minima is called lower envelop ($min[x(t)]$).

3. Determine the mean of the envelop, that is, the center point between local maxima and local minima at the specific time ($mean[x(t)] = \frac{max[x(t)]-min[x(t)]}{2}$).
4. Extract the intrinsic mode function (IMF) by subtracting the acquired signal with the mean of the envelop: ($IMF(t) = x(t) - mean[x(t)]$).
5. Iterate the process by using the residue signal. The residue signal is obtained by subtracting the original signal with the present IMF.

Arc sound signal was decomposed using the EMD algorithm into several components, called the IMF, which lies within a narrower frequency component compared with the original signal. In this case, each of the IMF is associated with different kinds of phenomena that elicited sound generation. Thus, in this study, only the IMF that was assumed to be a defect-related signal was selected to undergo the next stage of the analysis. In the next stage, the selected IMF will be analyzed using Hilbert transform (HT). According to [23], for an arbitrary signal $x(t)$, the HT $H[x(t)]$ can be determined by:

$$H[x(t)] = y(t) = \frac{PV}{\pi} \int_{-\infty}^{\infty} \frac{x(\tau)}{t - \tau} d\tau \tag{1}$$

where PV denotes the Cauchy principal value of the integral. Theoretically, $y(t)$ is a product of convolution of $x(t)$ with $1/\pi t$, which emphasizes the local properties of $x(t)$. By coupling the $x(t)$ and $y(t)$, the analytic complex signal $z(t)$ could be represented by Eq. 2.

$$z(t) = x(t) + iy(t) \tag{2}$$

Hence, instantaneous amplitude $a(t)$ can be determined by:

$$a(t) = \sqrt{x^2(t) + y^2(t)} \tag{3}$$

Table 1 MIG welding parameters

Specimen	Voltage (V)	Current (A)	Welding speed (mm/s)	Shielding gas (Argon) Flowrate (L/min))
1	24	200	5	15
2	24	170	3	7.5
3	23	165	4	10

and phase function of $z(t)$ can be written as:

$$\phi(t) = \arctan \frac{y(t)}{x(t)} \quad (4)$$

Meanwhile, the instantaneous frequency (IF) can be determined by:

$$IF = \frac{d(\phi(t))}{dt} \quad (5)$$

Basically, if all IMFs are considered for HT analysis, then the acquired signal $x(t)$ can be expressed as follows,

$$x(t) = \operatorname{Re} \left\{ \sum_{j=1}^n a_j(t) e^{i \int \omega_j(t) dt} \right\} \quad (6)$$

In Eq. 6, Re is the real part, whereas a_j and ω_j represent the instantaneous amplitude and IF of the j th IMF, respectively. If Eq. 6 is expanded in Fourier representation, then the equation turns into

$$x(t) = \operatorname{Re} \left\{ \sum_{j=1}^n a_j e^{i \omega_j t} \right\} \quad (7)$$

where both a_j and ω_j are constants. Equations 6 and 7 differ because in Eq. 6 the amplitude and frequency modulation can be distinctly observed with IMF expansion, thereby significantly overcoming the limitation of constant amplitude and fixed-frequency of the conventional Fourier expansion. Moreover, the amplitude and frequency modulation are significantly more noticeable if only selected IMFs undergo HT analysis. In essence, the frequency–time distribution of the amplitude is nominated as the Hilbert amplitude spectrum, $H(\omega, t)$ and its marginal spectrum, $h(\omega)$, can be expressed as follows

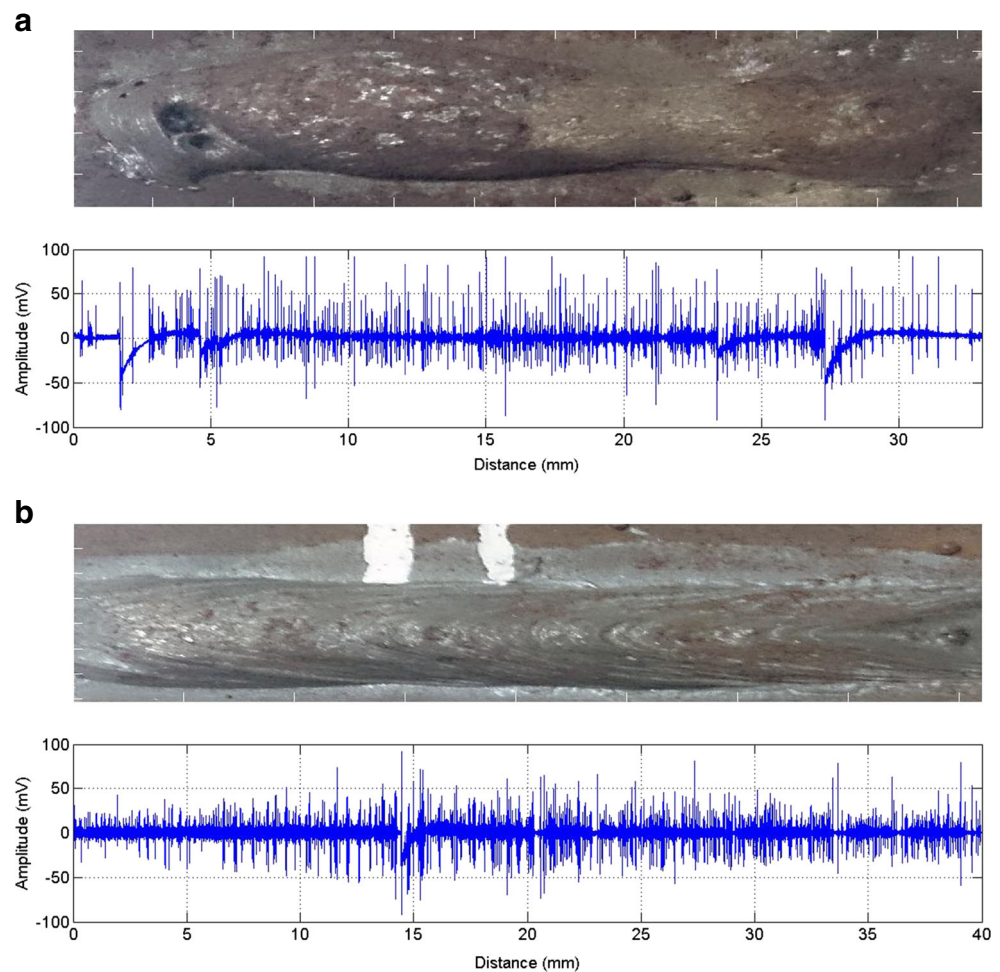
$$h(\omega) = \int_0^T H(\omega, t) dt \quad (8)$$

3 Result and discussion

3.1 Acquired sound signal

Figure 2a, b shows the distance domain plot of arc sound signals acquired during the welding process of specimens

Fig. 2 Sound signal acquired from the MIG welding process of **a** specimen 1 and **b** specimen 2



1 and 2, respectively. In this paper, the results for specimen 3 were not presented because neither defects nor any uncertainties were found in both the image and arc sound signal of specimen 3. Figure 2a shows noticeable uncertainties of sound amplitude detected from 2 to 5 mm from the starting point. The image of weld bead confirmed the presence of visible surface pores in this region. By contrast (in the same figure), an unexplained non-stationary behavior of sound amplitude can be observed at around 27 mm from the initial point. In specimen 2 (Fig. 2b), a similar phenomenon also appeared at around 14 mm from initial point. In both results, both non-stationary parts were barely noticeable. Meanwhile, the weld bead images in both figures did not indicate the existence of defects around this area.

3.2 Hilbert-Huang transform

As observed in the previous section, the acquired sound signal did not provide a clear or significant indication of the existence of any defects at certain regions, because of the random behavior and large amount of noise interrupting the signal. Consequently, the signal was decomposed into several components that lied within a narrower frequency to reduce the noise. Decomposition of the acquired sound signal was done through EMD analysis, and the decomposed result was called IMF. This process promoted a significant way to eliminate noise by only considering defect-related IMFs for the next process.

Figure 3a–d respectively shows the IMF 5, IMF 7, IMF 8, and IMF 11 of the decomposed sound signal from specimen 1. Among these IMFs, IMF 8 showed a very clear transient pattern at 2, 5, 23, and 27 mm from the initial welding point. The same phenomenon was also found at around 15 mm from the initial welding point in IMF 10 for specimen 2 (Fig. 4). According to Robert [24], during the welding process, insoluble ambient air is trapped within the weld pool as a result of the occurrence of Marangoni force, which creates a downward convection pattern. Consequently, the insoluble air turns into pores. Thus, it could be assumed that the presence of transient phenomena in the IMF was strongly related to the occurrence of Marangoni force.

By looking into the possibility of obtaining signs of subsurface pores, IMF 8 from specimen 1 and IMF 10 from specimen 2 were selected for the next analysis. Figures 5 and 6 showed the Hilbert spectra (HS) for IMF 8 from specimen 1 and IMF 10 from specimen 2, respectively. The HS in both figures were plotted together with the image of the weld bead. Overall, the region with increased energy amplitude was definitely the region where the subsurface pores existed on or underneath the weld bead. For instance, a deeper look into the image of the weld bead, as well as the results of the HS of IMF 8 from specimen 1 in Fig. 5a, b, indicated the presence of visible gas pores on the

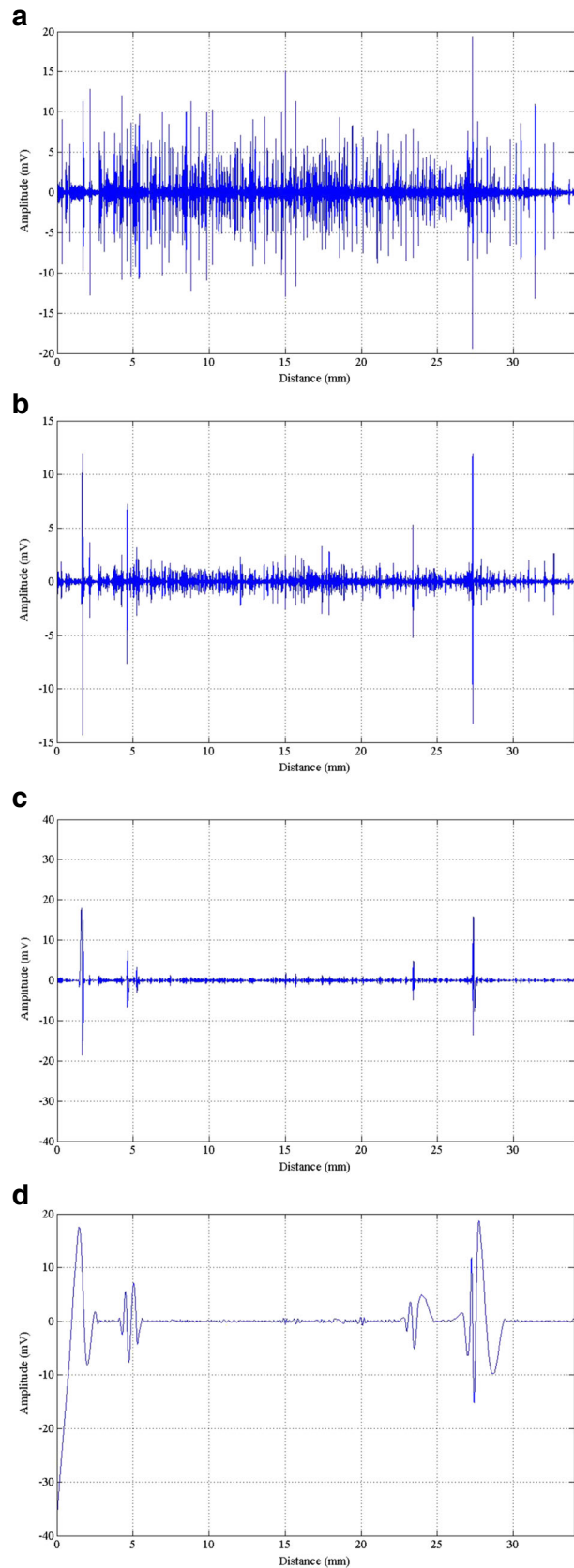


Fig. 3 Intrinsic mode function (IMF) of specimen 1 **a** IMF 5, **b** IMF 7, **c** IMF 8, and **d** IMF 11

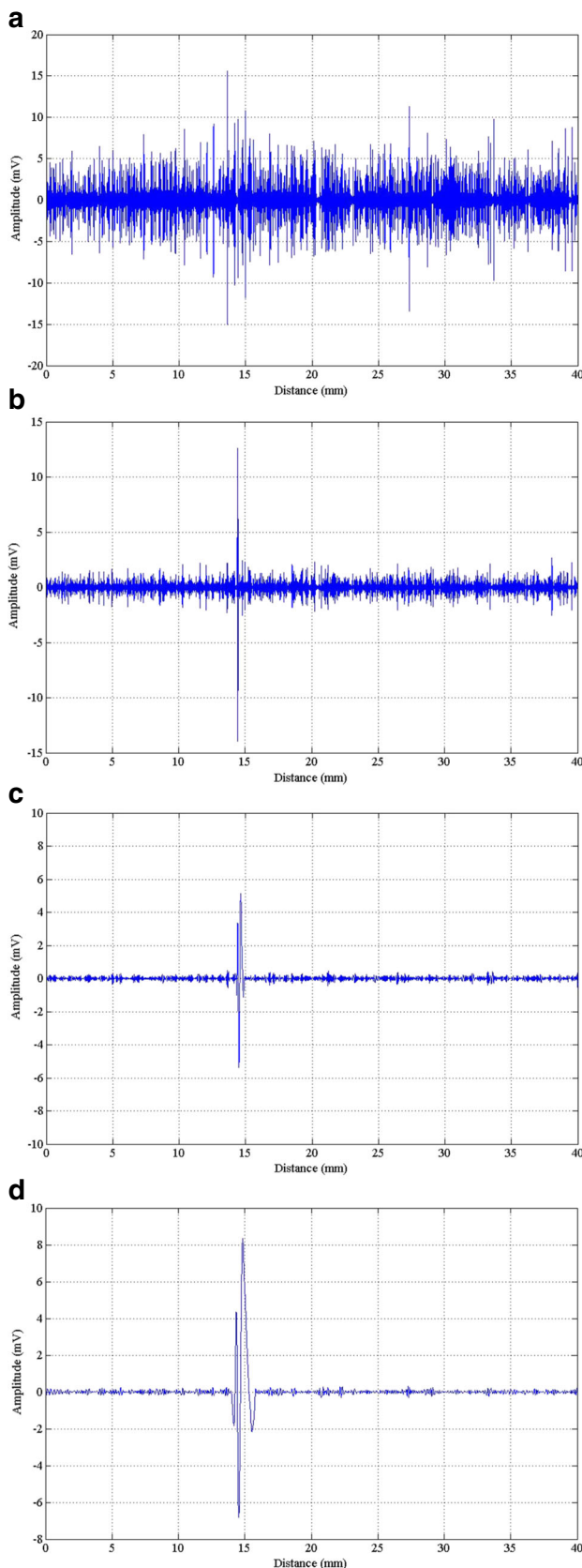


Fig. 4 Intrinsic mode function (IMF) of specimen 2 **a** IMF 5, **b** IMF 7, **c** IMF 10, and **d** IMF 11

surface around 2 to 5 mm from the initial point. Although no defects were detected on the surface, the initial unexplained energy amplitude increments observed at around 23 and 27 mm from the initial point indicated the presence of subsurface pores, which were found at 2.84 and 4.15 mm underneath the surface in both regions after the specimens were grounded (Fig. 5c, d, respectively). A similar result was found in specimen 2, which led to the detection of pores located at around 15 mm from the starting point and at 4.87 mm underneath the surface (Fig. 6).

The results in both Figs. 5a and 6a showed high-energy amplitudes from 10.02 to 70.14 Hz and 10.02 to 50.4 Hz for specimens 1 and 2, respectively. Theoretically, any force that occurs during the molten metal transfer process affects the behavior of the weld pool oscillation [24]. Thus, it could be estimated that the frequency range in both Figs. 5a and 6) are close to the natural oscillation frequency of the weld pool, and the occurrence of high-energy amplitude at that instant was due to Marangoni force. To confirm the statements, the natural oscillation frequency of the weld pool was analyzed using the Xiao-den and Ouden [25] model. The natural oscillation frequency of a weld pool for a partial penetrate case can be determined by using the following equations:

$$f_{mode\ 1} = 5.84 \left(\frac{\gamma}{\rho} \right)^{\frac{1}{2}} D_{eq}^{-\frac{3}{2}} \quad (9)$$

$$f_{mode\ 2} = 3.37 \left(\frac{\gamma}{\rho} \right)^{\frac{1}{2}} D_{eq}^{-\frac{3}{2}} \quad (10)$$

In Eqs. 9 and 10, γ , ρ , and D_{eq} denote the surface tension, density of liquid steel, and equivalent diameter, respectively. Primarily, the equivalent diameter of the weld pool D_{eq} calculation involves parameters, such as pool length L_t and pool width W_t , of an elliptic weld pool, as described in Eq. 11:

$$D_{eq}^2 = W_t \cdot L_t \quad (11)$$

To obtain the natural oscillation frequency value by using Eq. 10, the values for the liquid steel density, ρ , and surface tension, γ , of carbon steel are needed. According to Subramaniam and White [26], liquid steel density was 6500 kg/m³ and the surface tension of E70RS carbon steel filler was 1.52 N/m. These values were used in the present work to calculate the natural oscillation frequency because the E70RS filler is similar to API 5L X70 steel in terms of chemical composition and strength. Moreover, the same type of filler was used in this work. By measuring the pool width W_t and pool length L_t from the specimen, the estimated natural oscillation frequency was obtained (Table 2). Owing to the polarity behavior of the utilized MIG welding machine, the weld pool was assumed to be vibrating in mode 2. Therefore, only frequencies from mode 2 were

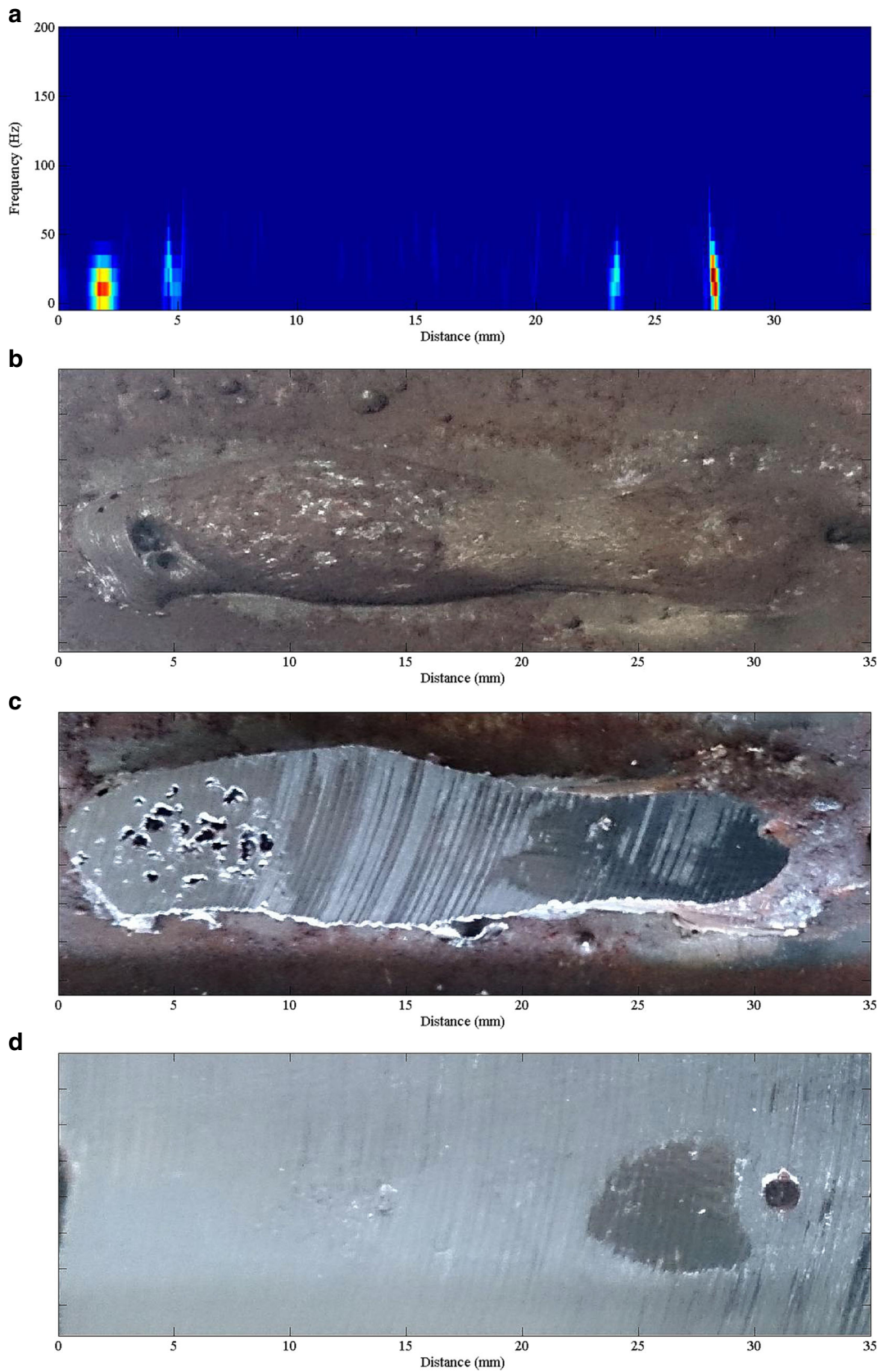


Fig. 5 Hilbert Huang analysis for specimen 1; **a** Hilbert spectrum, **b** original specimen, **c** grounded 2.84-mm depth, and **d** grounded 4.15-mm depth

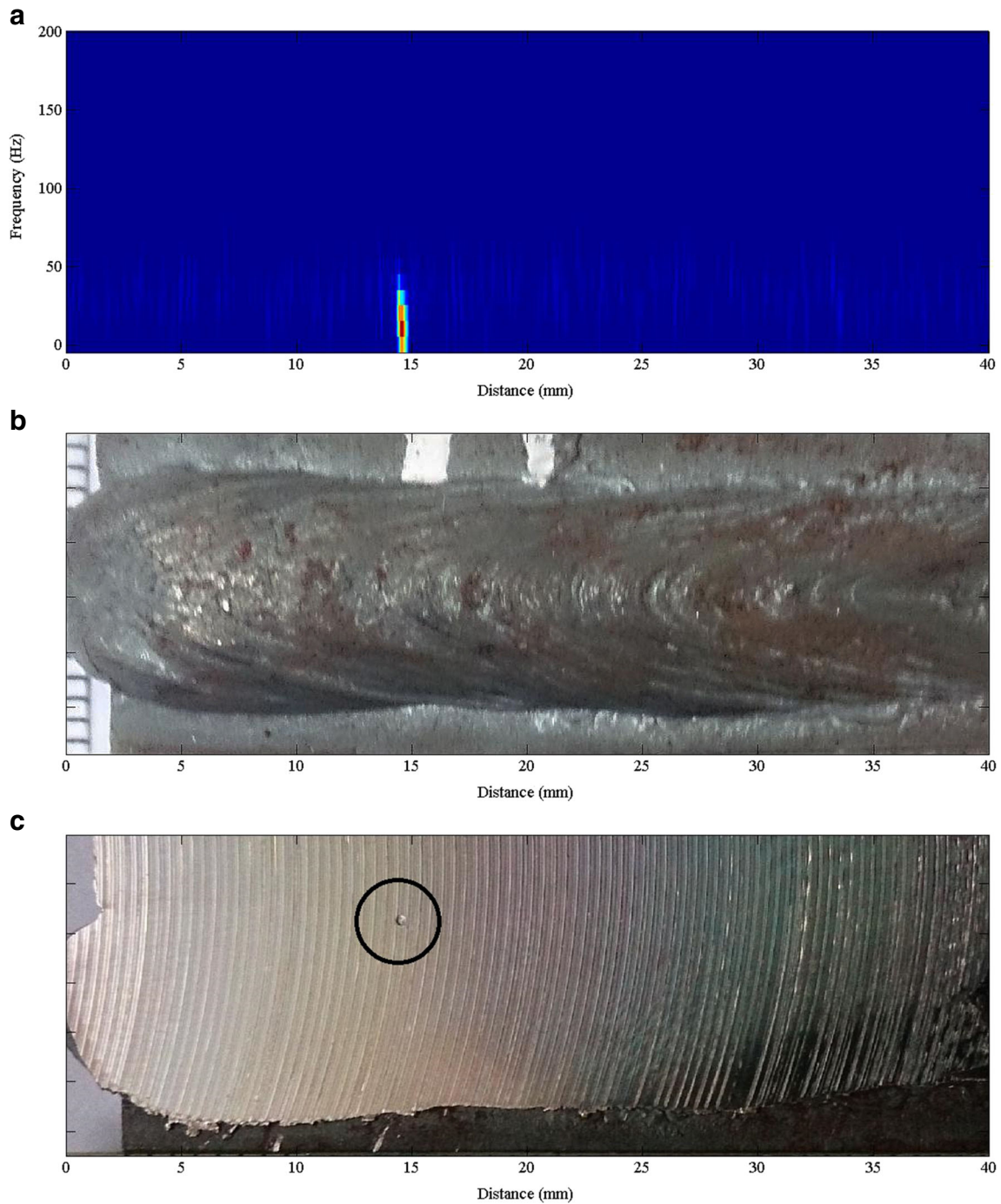


Fig. 6 Hilbert Huang analysis for specimen 2: **a** Hilbert spectrum, **b** original specimen, and **c** grounded 4.87-mm depth

calculated. The results in Table 2 showed that the frequency at the time when the energy amplitude increased in Figs. 5a and 6a were close to the calculated values of natural oscillation frequency, in which the mode shape can be referred in Fig. 7. These findings indicated that the information on IF provided in the HS had given the significant information on

Table 2 Natural oscillation frequency of the weld pool for specimen 1 and 2 under mode 2

Specimen	pool length L_f (mm)	Pool width W_f (mm)	Mode 2 (Hz)
1	9	7	72.87
2	12	8	53.13

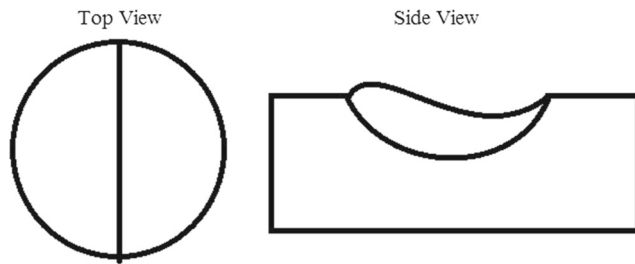


Fig. 7 Weld pool oscillation (for half penetration) under mode 2

the weld pool oscillation condition, which can be referred to detect any presence of porosity underneath the weld bead.

4 Conclusion

The results of this study showed that sound signal was successfully acquired during the MIG welding process of an API 5L X70 gas pipeline. Although some uncertainties in the raw signal pattern can provide signs of defects at certain locations, these signals did not give significant clues on the existence of subsurface defects, because signal uncertainties were difficult to observe in some cases. After the signal underwent HHT analysis, the results showed a significant pattern of energy amplitude at the region where both surface and subsurface pores were present. In addition, the frequency values in areas with defects were close to the estimated weld pool oscillation frequency calculated based on the data in literature. Thus, the HS plot can provide information on the presence of pores by observing the energy amplitude values at the natural oscillation frequency of a weld pool. In other words, the weld pool status can be monitored using HS. In conclusion, porosity underneath the weld bead can be detected using the acquired arc sound signal. Moreover, HHT analysis of the acquired sound significantly assisted in revealing the existence of defects owing to the decomposition process through the EMD method that simplified the filtering process by revealing the damage-related IMFs. The location of defects can be determined through observation of the oscillation behavior of weld pool using HS.

The results obtained in this work demonstrated the feasibility of using sound signal to detect subsurface defects during the welding process with the aid of a signal processing method. Hence, this study would facilitate the development of an online welding defect detection system to detect any types of defect during the welding process.

Acknowledgments This project is supported by the Universiti Malaysia Pahang Internal Research Grant (RDU130340).

References

- Aljaroudi A, Khan F, Akinturk A, Haddara M, Thodi P (2015) Risk assessment of offshore crude oil pipeline failure. *J Loss Prev Process Ind* 37:101–109. doi:10.1016/j.jlp.2015.07.004
- Asl HM, Vatani A (2013) Numerical analysis of the burn-through at in-service welding of 316 stainless steel pipeline. *Int J Press Vessel Pip* 105–106:49–59. doi:10.1016/j.ijpvp.2013.03.002
- Jha AK, Manwatkar SK, Narayanan PR, Pant B, Sharma SC, George KM (2013) Failure analysis of a high strength low alloy 0.15C–1.25Cr–1Mo–0.25V steel pressure vessel. *Case Stud Eng Fail Anal* 1(4):265–272. doi:10.1016/j.csefa.2013.09.004
- Hval M, Lamvik T (2015) Parameters affecting the weld defect acceptance criteria of clad submarine pipelines installed by S-lay or reel-lay. *Eng Fail Anal* 58:394–406. doi:10.1016/j.engfailanal.2015.07.003
- Carlson M, Johnson JA, Kunerth DC (1992) Control of GMAW: detection of discontinuities in the weld pool. *NDT E Int* 25: 44
- Ulbrich D, Kowalczyk J, Jósko M, Selech J (2015) The analysis of spot welding joints of steel sheets with closed profile by ultrasonic method. *Case Stud Nondestruct Test Eval* 4:8–14. doi:10.1016/j.csndt.2015.09.002
- Bentley PG, Dawson DG, Prine DW (1982) An evaluation of acoustic emission for the detection of defects produced during fusion welding of mild and stainless steels. *NDT Int* 15(5):243–249. doi:10.1016/0308-9126(82)90033-5
- Yu J, Ziehl P, Matta F, Pollock A (2013) Acoustic emission detection of fatigue damage in cruciform welded joints. *J Constr Steel Res* 86:85–91. doi:10.1016/j.jcsr.2013.03.017
- Valavanis I, Kosmopoulos D (2010) Multiclass defect detection and classification in weld radiographic images using geometric and texture features. *Expert Syst Appl* 37(12):7606–7614. doi:10.1016/j.eswa.2010.04.082
- Alaknanda, Anand RS, Kumar P (2006) Flaw detection in radiographic weld images using morphological approach. *NDT & E Int* 39(1):29–33. doi:10.1016/j.ndteint.2005.05.005
- Vilar R, Zapata J, Ruiz R (2009) An automatic system of classification of weld defects in radiographic images. *NDT & E Int* 42(5):467–476. doi:10.1016/j.ndteint.2009.02.004
- Kasban H, Zahran O, Arafa H, El-Kordy M, Elaraby SMS, Abd El-Samie FE (2011) Welding defect detection from radiography images with a cepstral approach. *NDT & E Int* 44(2):226–231. doi:10.1016/j.ndteint.2010.10.005
- Yu H, Xu Y, Song J, Pu J, Zhao X, Yao G (2015) On-line monitor of hydrogen porosity based on arc spectral information in Al–Mg alloy pulsed gas tungsten arc welding. *Opt Laser Technol* 70:30–38. doi:10.1016/j.optlastec.2015.01.010
- Zhang Z, Kannatey-Asibu E Jr, Chen S, Huang Y, Xu Y (2015) Online defect detection of Al alloy in arc welding based on feature extraction of arc spectroscopy signal. *Int J Adv Manuf Technol* 79:2067–2077. doi:10.1007/s00170-015-6966-9
- Wang Y, Zhao P (2001) Noncontact acoustic analysis monitoring of plasma arc welding. *Int J Press Vessel Pip* 78(1):43–47. doi:10.1016/S0308-0161(00)00085-5
- Huang W, Kovacevic R (2009) Feasibility study of using acoustic signals for online monitoring of the depth of weld in the laser welding of high-strength steels. *Proc Inst Mech Eng B J Eng Manuf* 2009(223):343–361
- Saad E, Wang H, Kovacevic R (2006) Classification of molten pool modes in variable polarity plasma arc welding based on

- acoustic signature. *J Mater Process Technol* 174(1–3):127–136. doi:[10.1016/j.jmatprotec.2005.03.020](https://doi.org/10.1016/j.jmatprotec.2005.03.020)
18. Grad L, Grum J, Polajnar I, Marko Slabe J (2004) Feasibility study of acoustic signals for on-line monitoring in short circuit gas metal arc welding. *Int J Mach Tools Manuf* 44(5):555–561. doi:[10.1016/j.ijmachtools.2003.10.016](https://doi.org/10.1016/j.ijmachtools.2003.10.016)
 19. Wang Y, Chen Q, Sun Z, Sun J (2001) Relationship between sound signal and weld pool status in plasma arc welding. *Trans Nonferrous Metals Soc Chin* 11(01):54–57
 20. You DY, Gao XD, Katayama S (2014) Review of laser welding monitoring. *Sci Technol Weld Join* 19(3):181–201. doi:[10.1179/1362171813Y.0000000180](https://doi.org/10.1179/1362171813Y.0000000180)
 21. Huang W, Kovacevic R (2011) A neural network and multiple regression method for the characterization of the depth of weld penetration in laser welding based on acoustic signatures. *J Intell Manuf* 22(2):131–143. doi:[10.1007/s10845-009-0267-9](https://doi.org/10.1007/s10845-009-0267-9)
 22. Luo Z, Liu W, Wang Z, Ao S (2015) Monitoring of laser welding using source localization and tracking processing by microphone array. *Int J Adv Manuf Technol* 1–8. doi:[10.1007/s00170-015-8095-x](https://doi.org/10.1007/s00170-015-8095-x)
 23. Huang NE, Shen Z, Long SR, Wu ML, Shih HH, Zheng Q, Yen NC, Tung CC, Liu HH (1998) The empirical mode decomposition and Hilbert spectrum for nonlinear and nonstationary time series analysis. *Proc Roy Soc London A* 454(1998):903–995
 24. Messler RW Jr (2004) *Principle of welding: process, physics, chemistry and metallurgy*. Wiley VCH Verlag GmbH & Co., Singapore
 25. Xiao YH, Ouden GD (1993) Weld pool oscillation during GTA welding of mild steel. *Weld J (Miami)* 72
 26. Subramaniam S, White DR (2001) Effect of shield gas composition on surface tension of steel droplet in a gas-metal-arc welding arc. *Metall Mater Trans B* 32(2001):313–318